Available online at www.sciencedirect.com
ScienceDirect
Continental Shelf Research 28 (2008) 561–573
CONTINENTAL SHELF RESEARCH
www.elsevier.com/locate/csr

Benefit of nesting a regional model into a large-scale ocean model instead of climatology. Application to the West Florida Shelf

A. Barth*, A. Alvera-Azcárate, Robert H. Weisberg

University of South Florida, College of Marine Science, 33701 St. Petersburg, FL, USA

Received 20 February 2007; received in revised form 5 October 2007; accepted 9 November 2007
Available online 21 November 2007

Abstract

The impact of open boundary conditions on the dynamics and accuracy of a regional West Florida Shelf model is addressed. A ROMS-based model nested in monthly climatological temperature and salinity and in the North Atlantic HYCOM model is implemented. The model results of these nesting implementations are compared to altimetry, *in situ* temperature time series, and ADCP and high-frequency (HF) radar currents. A significant improvement of the model results is found using the boundary conditions of the HYCOM model over the climatology. The ageostrophic nature of the LC is studied and the benefit using the velocity and surface elevation boundary conditions is shown.

Keywords: Nested model; Open boundary conditions; Shelf circulation; West Florida Shelf

1. Introduction

Several large-scale operational ocean modeling systems have been developed (e.g. ECCO (Estimating the Circulation and Climate of the Ocean; Stammer and Chassignet, 2000), FOAM (Forecasting Ocean Assimilation Model; Bell et al., 2000), HYCOM (Hybrid Coordinate Ocean Model; Chassignet et al., 2007), MERCATOR (Bahurel et al., 2004), MFS (Mediterranean Forecast System; Demirov et al., 2003), NCOM (Navy Coastal Ocean Model; Barron et al., 2006), TOPAZ (Towards an Operational Prediction system for the North Atlantic European coastal Zones; Bertino et al., 2006)). One of the objectives of these systems is to provide, among other products, boundary and initial conditions for regional ocean models.

However, since deep-ocean currents are constrained to a large extent by the bathymetry, their direct impact on the shelf may be limited. Here, we examine the influence of the deep-ocean currents on the realism of a shelf model using the initial and boundary conditions from the large-scale ocean general circulation North Atlantic HYCOM (NAT HYCOM) and assess this relative to initial and boundary conditions from climatology. Both model nesting strategies are applied to the West Florida Shelf (WFS).

The WFS is generally wide, extending about 200 km to the shelf break except in the DeSoto Canyon region where the shelf is relatively narrow (Fig. 1). The currents on the shelf are mainly driven by winds and atmospheric heat fluxes (e.g. Weisberg et al., 2001; He and Weisberg, 2002b). Northerly (southerly) winds tend to produce upwelling (downwelling) along the west Florida coast (Weisberg et al., 2000). Since the surface heat fluxes control the stratification, the Ekman dynamics are also influenced by the atmospheric heat input (e.g. Weisberg et al., 2001).

Beyond the shelf break, the variability is mainly generated by the loop current (LC). The LC derives from the branch of the western boundary current entering the Gulf of Mexico through the Yucatan Channel. It undergoes an anticyclonic loop before exiting the Gulf of Mexico through the Florida Straits to initiate the Gulf Stream. Instabilities modulate the path of the LC and lead to the shedding of large anticyclonic eddies that propagate westward in the Gulf of Mexico. Smaller eddies are also

*Corresponding author.
E-mail addresses: a.barth@ulg.ac.be, barth.alexander@gmail.com (A. Barth).

0278-4343/$ - see front matter © 2007 Elsevier Ltd. All rights reserved.
doi:10.1016/j.csr.2007.11.004

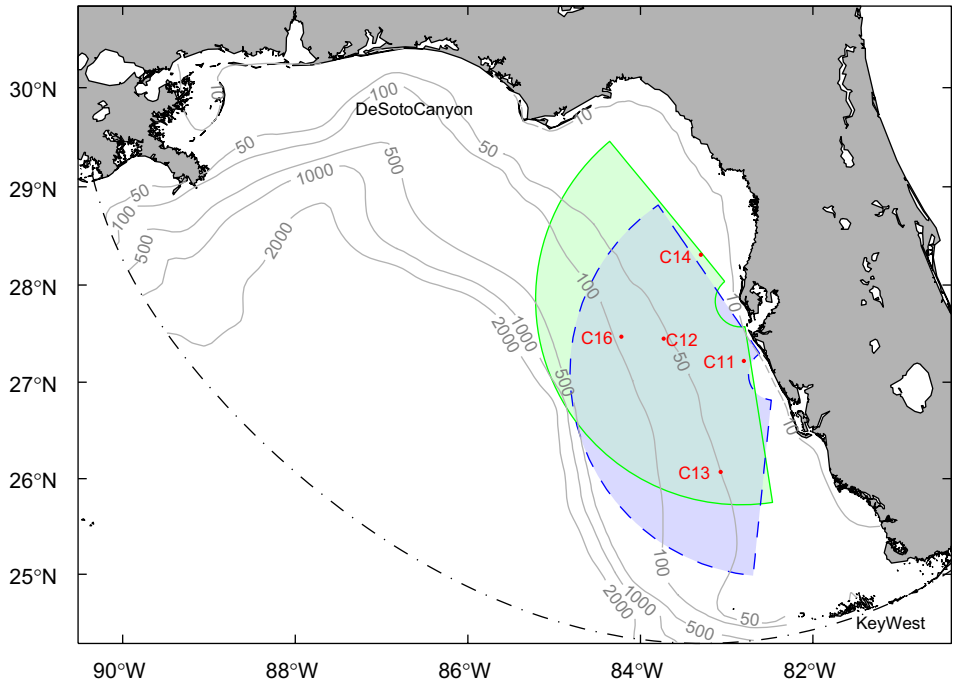

Fig. 1. The West Florida Shelf. The dash-dotted line shows the open boundary of the WFS ROMS domain and isolines represent the depth of the model bathymetry (in m). The regions in green and blue delimited by the solid and dashed lines represent the coverage of Redington and Venice CODAR stations, respectively. The dots show the locations of *in situ* measurements used for validation along with their names.

generated at the eastern flank of the LC moving towards the WFS. Topographic Rossby waves moving northward along the shelf break are produced when the LC or its eddies contact the shelf slope (Hetland et al., 1999). If such a contact occurs near Dry Tortugas where the isobaths converge, then currents over the entire WFS may be generated. Through this mechanism, and in combination with local forcing, deep water can be advected onto the shelf (He and Weisberg, 2003b; Weisberg and He, 2003). A general review of the WFS circulation can be found in Weisberg et al. (2005).

Several regional model studies have been conducted on the WFS. For instance, the Princeton Ocean Model (POM) of Blumberg and Mellor (1987) was used to compute the wind and buoyancy forced circulations (He and Weisberg, 2002b). In He and Weisberg (2003a), an idealized LC was introduced by imposing sea level at the open boundary. Tides were simulated with POM in a similar configuration (He and Weisberg, 2002a). Halliwell et al. (2005) tested the HYCOM as a regional model and stressed the importance of the choice of the vertical coordinate and the mixing scheme.

Previous studies conclude that with the exception of specifically tailored events, the impact of the LC on the inner shelf is limited (e.g. He and Weisberg, 2003b). Therefore it is unclear if the model performance on the shelf can be improved through model nesting and through a more realistic LC. In this paper, we assess the influence of the open boundary on the shelf circulation using time series of *in situ* temperature, and ADCP and High Frequency (HF)-Radar currents. We will address if velocity and elevation boundary information, which can be provided by an ocean general circulation model (OGCM) but which are not directly available from climatological temperature and salinity estimations, have an impact on the shelf.

Section 2 outlines the model experiments with the mentioned different boundary conditions. The large-scale differences between the model results are discussed in Section 3. Section 4 studies the model differences on the shelf comparing the model results to *in situ* data. We finish with conclusions and summarize our findings in Section 5.

2. Description of the model experiments

The ROMS model (Regional Ocean Modeling System; http://www.myroms.org) solves the three-dimensional, free surface, hydrostatic, primitive equations (Shchepetkin and McWilliams, 2005). The WFS model domain is shown in Fig. 1. The horizontal resolution of its curvilinear grid ranges from 4 km near the coast to 10 km near the open boundary. The vertical is discretised in 32 levels using the s-coordinate.

The atmospheric forcings include air temperature, relative humidity, cloud fraction and short-wave radiation from Navy Operational Global Atmospheric Prediction System (NOGAPS) and an optimal interpolated (OI) wind product combining NCEP NAM winds (National Centers for Environmental Prediction, North American Mesoscale Model) with *in situ* wind measurements (He et al., 2004). The model SST is relaxed to a cloud-free optimal interpolated SST (He et al., 2003) based on AVHRR (Advanced Very High Resolution Radiometer), GOES

(Geostationary Operational Environmental Satellites), MODIS (MODerate Resolution Imaging Spectroradiometer) and TMI (TRMM Microwave Imager) as described in Barnier et al. (1995). A 1 °C difference between model SST and optimal interpolated SST would result in a correcting heat flux of 47 W m^{-2}.

In order to emphasize the role of the boundary conditions on the WFS model, we conducted the following three model experiments:

(1) *WFS ROMS nested in temperature and salinity climatology*: The monthly temperature and salinity climatology of Ruoying He (personal communication), which is based on the data set of Levitus and Boyer (1994) and Levitus et al. (1994), is used and bi-linearly interpolated in space on the model grid. For the elevation we used a zero-gradient boundary condition and for the velocity, temperature and salinity we used a radiative boundary condition (Marchesiello et al., 2001). Additionally, the model temperature and salinity are nudged towards the climatological values with a spatially variable relaxation time scale. At the open boundary, the relaxation time scale ($1/c_j$) is shortest with $\tau = 1$ day. For other grid points the relaxation time scale is given by

$$\begin{aligned} c_j &= \frac{1}{2\tau}\left(1+\cos\left(\frac{j\pi}{n}\right)\right) \quad \text{for } j \leqslant n, \\ c_j &= 0 \qquad\qquad\qquad\qquad\quad \text{elsewhere.} \end{aligned} \tag{1}$$

The index j is the distance from the open boundary in model grid points. The width of this relaxation zone (n) is 10 grid points. The model is initialized from a one-year model spin-up using also climatological boundary conditions.

This type of boundary conditions have been applied successfully in a regional model implementation of the ROMS in the US West Coast using climatological boundary values and it has been shown to be stable and accurate (Marchesiello et al., 2001). Now these boundary conditions are applied to nest the WFS ROMS in the NAT HYCOM.

(2) *WFS ROMS nested in NAT HYCOM temperature and salinity*: The daily temperature and salinity from the NAT HYCOM model (Chassignet et al., 2007) are used as boundary conditions in this experiment. These tracers are interpolated in space and time and the nesting procedure and the used parameters are the same as the previous experiment. For the initialization we used the interpolated tracers, velocity and elevation from HYCOM on 1 January 2004.

(3) *WFS ROMS fully nested in NAT HYCOM*: Not only temperature and salinity are used in this experiment, but also the elevation and velocity of NAT HYCOM. The elevation and barotropic velocity are imposed at the boundary as a Chapman (1985) and Flather (1976) boundary conditions, respectively. The radiative boundary conditions are applied to the tracers and to the baroclinic velocity. In addition to those boundary conditions, the model temperature, salinity and velocity (barotropic and baroclinic) are relaxed to the corresponding NAT HYCOM fields. The relaxation time scale is given by Eq. (1) with $\tau = 0.1$ days. The model is initialized with the same initial conditions as the previous experiment.

The 1st nesting experiment aims to simulate the WFS without using any information from a large-scale model. This simulation will be compared to the 3rd nesting scenario which uses all available information from the large-scale model to drive a regional application. Differences between the 1st and 3rd simulations are therefore due to two factors: (i) different temperature and salinity values at the boundary and (ii) additional boundary conditions of velocity and elevation. The 2nd experiment is introduced to assess the relative importance of both factors. The difference between experiments 1 and 2 is the result of using a more realistic temperature and salinity from HYCOM instead of climatology and the difference between simulations 2 and 3 shows the impact of the velocity and elevation boundary conditions.

Boundary conditions from a monthly climatology are by construction less energetic than boundary conditions obtained from an eddy-resolving circulation model sampled at a daily frequency. The later boundary conditions increase necessarily the variability of the nested model. The impact of this increased variability on the RMS error of the model compared to observations can be expressed as (Taylor, 2001; Alvera-Azcárate et al., 2007)

$$RMS^2 = b^2 + \sigma_m^2 + \sigma_o^2 - \sigma_m \sigma_o R, \tag{2}$$

where RMS, b and R are the RMS error, the bias and the correlation between model and observations, respectively, and σ_m and σ_o are the standard deviation of model and observations, respectively. A model with a lower variability can thus have a better RMS than a model with more realistic variability if the correlation is poor. The present study aims to assess if a more realistic and more variable boundary condition is beneficial to a nested model when its accuracy is assessed in terms of RMS error relative to observations.

Different relaxation strengths and relaxation zone widths were tested. We present only the results leading to the simulation that most closely represents the observations.

3. Large-scale circulation

The LC is the main large-scale feature in the WFS domain. Fig. 2 shows the mean sea surface height (SSH) on April 2004 for the three model configurations and for the AVISO sea surface height anomaly (Ducet et al., 2000) added to the MICOM mean SSH (Chassignet and Garraffo, 2001) all averaged over the same time period. April 2004 was chosen because the LC was very stable during this month (i.e. there was no eddy shedding and the LC trajectory was stable). *A priori*, the model forced with

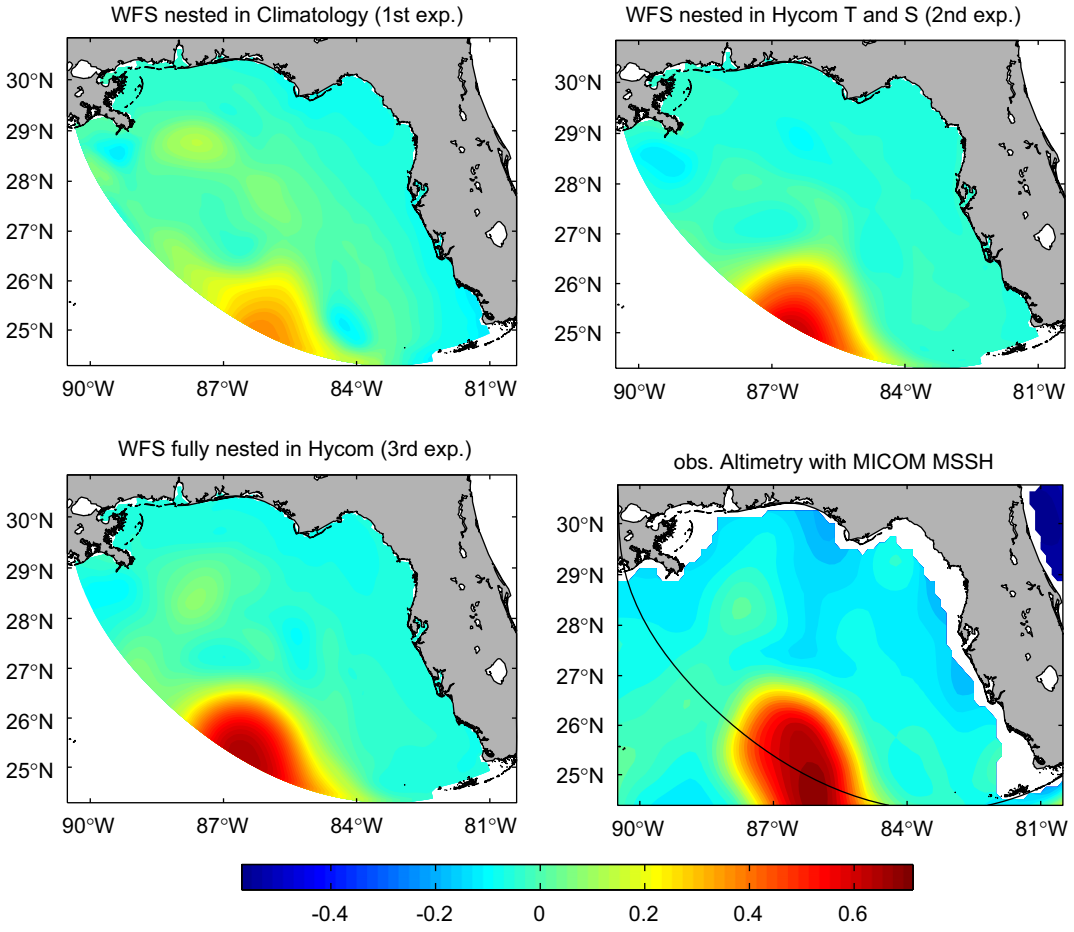

Fig. 2. Mean sea surface height (in m) on April 2004 from the model (first three panels) and observations (lower right panel).

climatology should be able to reproduce the deep ocean currents in this situation. The SSH gradients are indicative of the LC velocity and the LC SSH maximum is related to LC volume transport, since the SSH is a proxy for the stream function of the upper ocean. In the model run with climatological forcings, the LC is too weak. Its SSH maximum is, with 0.3 m (upper left panel of Fig. 2), significantly lower than the maximum SSH derived from altimetry and MICOM (0.70 m; lower right panel of Fig. 2).

By using HYCOM temperature and salinity (upper right panel of Fig. 2), the model is able to represent the LC much more realistically. In particular the maximum SSH (0.62 m) is much closer to the altimetry, but is still too small. The NAT HYCOM assimilates altimetry observations and the WFS ROMS model benefits from those improved boundary conditions. By using also NAT HYCOM velocity and elevation (lower left panel of Fig. 2), the LC strength (0.66 m of maximum SSH) comes closest to the observations. This indicates that the density field alone is not sufficient to completely represent the LC transport.

The velocity and elevation from NAT HYCOM is even more important after an eddy shedding as it can be seen in Fig. 3 where the mean SSH for the three model simulations and observations for October 2004 are shown. The inertial forces increase the curvature of the LC, and the advection of momentum near the boundary plays an increasingly important role. The WFS ROMS model fully nested in HYCOM (lower left panel of Fig. 3) describes more accurately the shape and intensity of the LC and the LC eddy NW of the WFS domain. For completeness, the WFS solution with climatological forcing is also shown (upper left panel of Fig. 3). In this experiment, a realistic eddy shedding is certainly not expected, but the strength of the LC is again misrepresented using climatological forcings. Also, the model with climatological forcing shows a strong cyclonic circulation. The density gradient in the climatology appears not strong enough to sustain a LC with a realistic strength and path. Since the LC trajectory is variable, with a northward excursion ranging between 23°N to 28°N (Leben, 2005), the climatology combining observations from multiple years produces inevitably low density gradients. Even if one is only interested in including a typical path and strength of a feature like the LC in a nested model, a climatology constructed by averaging out inter-annual variability appears to be insufficient. Traditionally, a climatology is defined as the error variance minimizing state and is obtained from optimal interpolation (this corresponds to the average of a sequence of co-located observations). If instead, a climatology is constructed as the most likely state of the LC

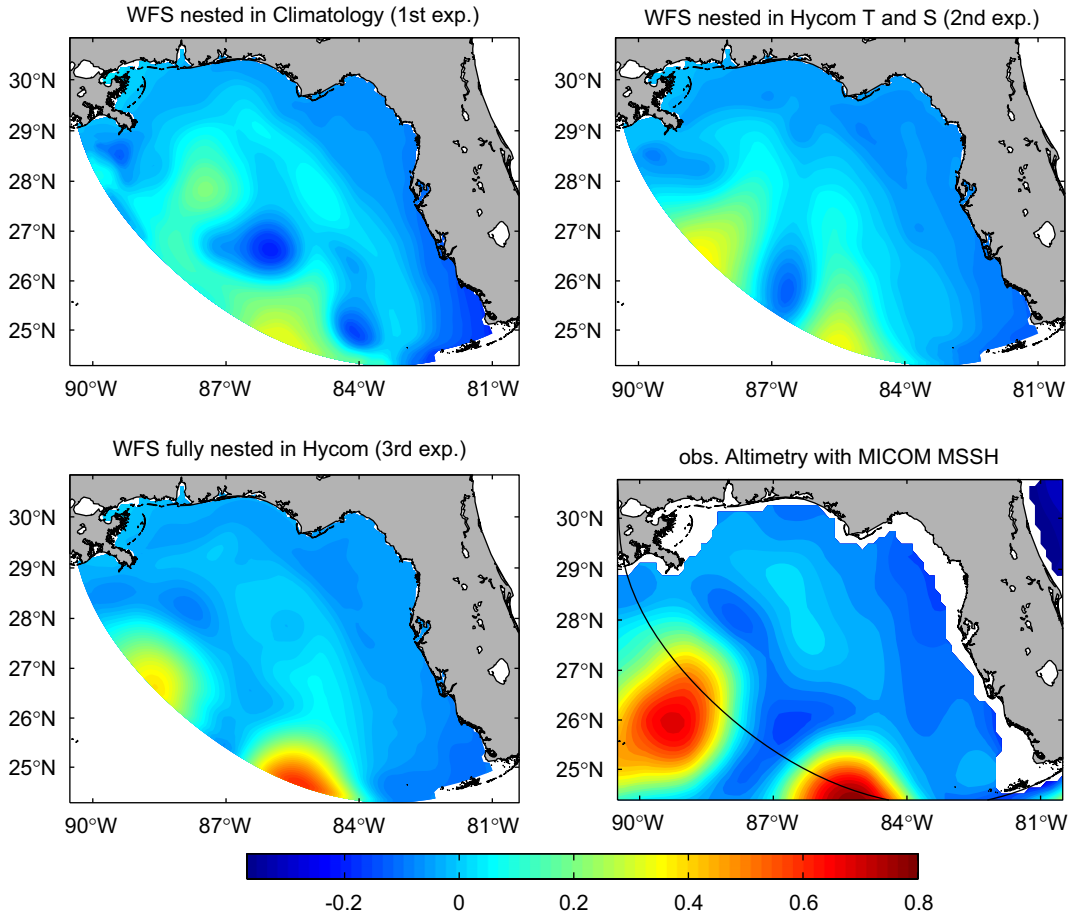

Fig. 3. Mean sea surface height (in m) on October 2004 from the model (first three panels) and observations (lower right panel).

(which corresponds to the mode of a sequence of observations) for a given month, gradients can be preserved and such climatology would probably be better suited for model nesting.

The time average of the model currents of experiments 2 and 3 at 100 m depth (about the mid-depth of the LC) reveals that the model experiment using only temperature and salinity from HYCOM has a weaker LC than the 3rd model experiment using also velocity and elevation. Since the 2nd experiment uses only temperature and salinity, the currents at the boundary are essentially adjusted geostrophically to the density field. The ageostrophic flow is thus not taken into account in this experiment. In order to assess the importance of the ageostrophic components, the RMS difference at 100 m depth between the model currents of experiment 3 (which is the closest to the real ocean) and the geostrophic currents based on the hydrostatic pressure of experiment 3 is computed:

$$RMS^2 = \frac{1}{T}\int_0^T (u-u_g)^2 + (v-v_g)^2\,\mathrm{d}t, \tag{3}$$

where u and v are the model velocity components and u_g and v_g are the geostrophic velocity components based on the model temperature, salinity and surface elevation. This RMS difference is shown in panel (a) of Fig. 4. In the LC, the model currents differ from the geostrophic currents by 0.25 m/s. The kinetic energy of this difference amounts to 20% of the average kinetic energy of the LC computed simply by

$$KE = \frac{1}{T}\int_0^T u^2 + v^2\,\mathrm{d}t. \tag{4}$$

The time-averaged RMS difference between model experiments 2 and 3 at 100 m depth is shown in panel (b) of Fig. 4. The overall structure and magnitude of the ageostrophic velocity components agrees with the RMS difference between the model simulations 2 and 3. The largest RMS differences in panel (b) are associated with the LC at the open boundary. These differences at the model boundary propagate inside of the model domain in form of eddies and filaments which are generated by the LC. By imposing the full velocity field at the model boundary, the ageostrophic flow components are included, which leads thus to a more realistic model simulation.

4. Shelf circulation

4.1. Temperature

The model results obtained by the three nesting configurations are compared with a series of moorings

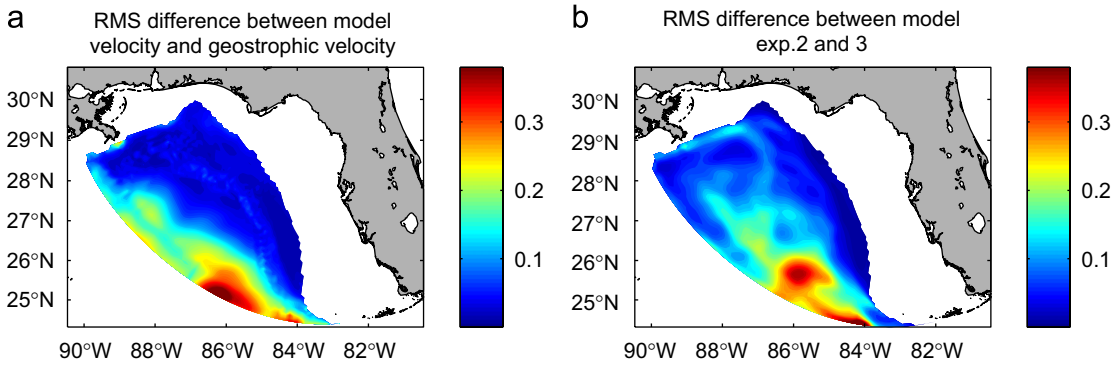

Fig. 4. Time-averaged RMS difference between model currents at 100 m and the geostrophic currents based on the model pressure for experiment 3 (panel a) and time-averaged RMS different between experiment 2 and 3 (panel b).

located on the WFS (see Fig. 1). At 1 m depth, the surface temperature time series of all model simulations are quantitatively similar due to the common heat flux forcing, and they are in good agreement with the observations at station C12 (Fig. 5). The model surface results were also compared at stations C14 and C16 (not shown) with a similar outcome. The surface properties on the shelf are thus largely determined by the surface boundary conditions and not by the open sea boundary conditions.

The model temperature at station C13 at mid-depth (10 m) are shown in Fig. 6. The model simulations are generally colder than the observed temperature. The analysis of the spatial temperature distribution revealed that this cold water originated from the deep ocean and is upwelled on shelf where the open boundary intersects the shelf-break. This issue is reduced when ROMS is fully nested in HYCOM instead of climatological forcings. Therefore the temperature of the model simulation fully nested in HYCOM is more realistic at depth than the model simulation with climatological forcings.

Fig. 7 shows the near-bottom (19 m) temperature at station C11. The model forced with climatology is too cold during summer and has the highest RMS error of all three model experiments. During summer, the model experiment forced with climatology develops an unrealistic southward coastal current which can be seen in Fig. 8. This current exits the model domain near Key West (Fig. 1) and is determined by the model boundary conditions. A persistent upwelling in the bottom Ekman Layer is associated with this current and therefore we observe this temperature bias in the model simulation with climatology. The best temperature time series is obtained with ROMS nested in HYCOM which shows a more realistic current variability as it will be discussed in the next section when comparing the model with ADCP data.

In order to assess the overall performance of the different nesting experiments compared to *in situ* temperature, the RMS errors at all available depths at stations C11, C12, C13, C14 and C16 were computed. The average model RMS error with climatology was 0.69 °C. This result is improved when HYCOM temperature and salinity are used as boundary conditions since the error is reduced to 0.62 °C. The best results, with an RMS error of 0.58 °C, were obtained with the model fully nested in HYCOM.

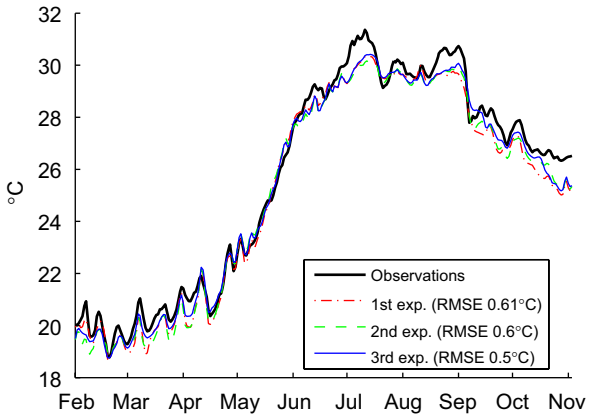

Fig. 5. Observed temperature time series of station C12 at 1 m depth and temperature of the WFS ROMS nested in climatology (1st exp.), WFS ROMS nested in NAT HYCOM temperature and salinity (2nd exp.) and WFS ROMS fully nested in NAT HYCOM (3rd exp.). Dates indicate the first day of each month.

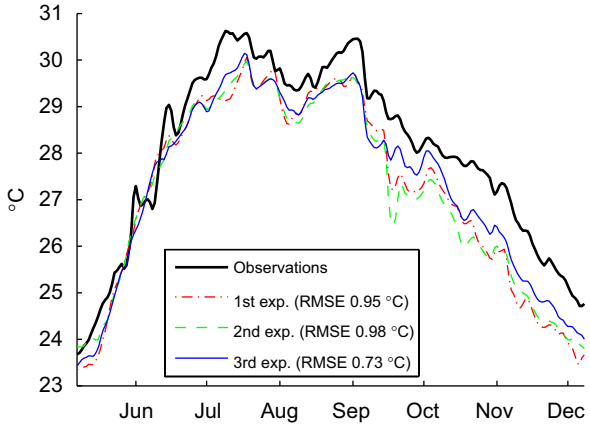

Fig. 6. Observed temperature time series of station C13 at 10 m depth and temperature of the WFS ROMS nested in climatology (1st exp.), WFS ROMS nested in NAT HYCOM temperature and salinity (2nd exp.) and WFS ROMS fully nested in NAT HYCOM (3rd exp.).

4.2. ADCP currents

The currents on the WFS are mainly driven by winds and buoyancy fluxes. All model configurations use the same atmospheric forcings and one can expect similar results for all cases. However, we noticed a persistent difference in terms of velocity RMS error. Fig. 8 shows the velocity time series for the entire simulation period at the surface as well as correlation (γ), phase error (ϕ), vector regression coefficient (r) and RMS error. These error measures are computed using the complex velocity w_n:

$$w_n = u_n + iv_n, \tag{5}$$

where u_n and v_n are the meridional and zonal velocity components, respectively. The subscript n is the time index. The RMS error and the complex correlation (e.g. Kundu and Allen, 1976) are given by

$$\mathrm{RMS} = \frac{1}{\sqrt{N}}\|w^m - w^o\|, \tag{6}$$

$$c = \frac{\langle w^m, w^o\rangle}{\|w^m\|\|w^o\|}. \tag{7}$$

The superscripts m and o refer to the model and observations, respectively, and N is the length of the time series. The scalar product and the norm are defined as usual by

$$\langle w^m, w^o\rangle = \sum_{n=1}^{N} \overline{w_n^m} w_n^o, \tag{8}$$

$$\|w\| = \sqrt{\langle w, w\rangle}. \tag{9}$$

The over-bar represents the complex conjugate. The complex correlation coefficient is decomposed in magnitude γ and phase error ϕ:

$$c = \gamma e^{i\phi}. \tag{10}$$

The vector regression coefficient, indicating whether the model under- or overestimates the observed currents, is computed by

$$r = \frac{|\langle w^m, w^o\rangle|}{\|w^o\|^2}. \tag{11}$$

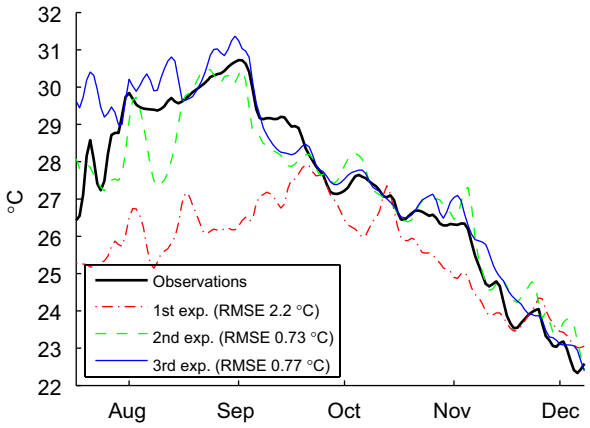

Fig. 7. Observed temperature time series of station C11 at 19 m depth and temperature of the WFS ROMS nested in climatology (1st exp.), WFS ROMS nested in NAT HYCOM temperature and salinity (2nd exp.) and WFS ROMS fully nested in NAT HYCOM (3rd exp.).

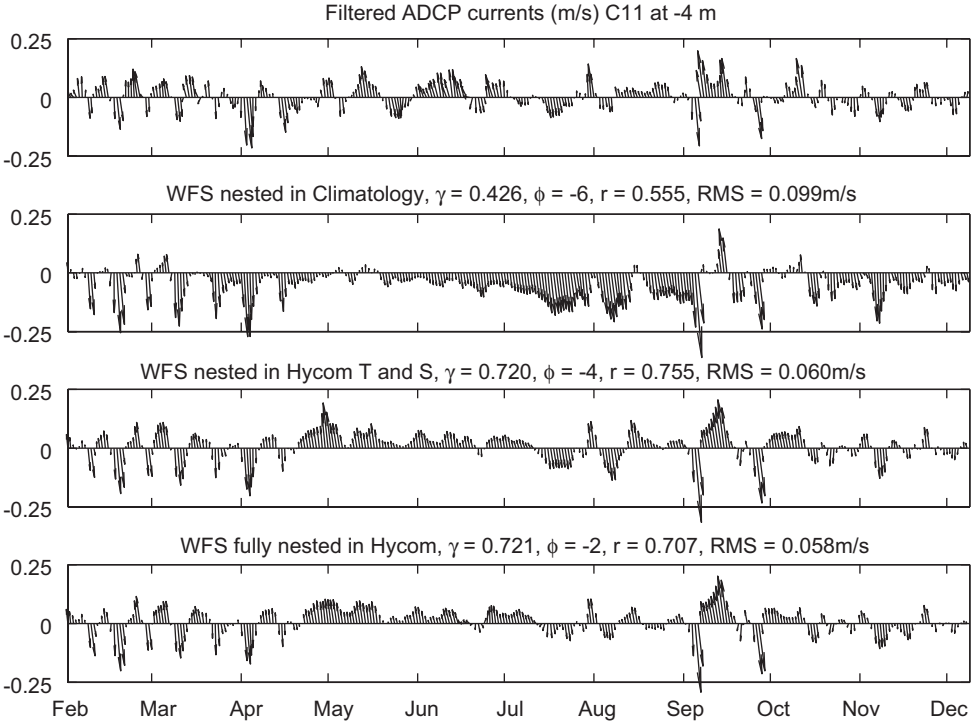

Fig. 8. Observed ADCP current time series (24-h low-pass filtered) of station C11 at 4 m depth and temperature of the WFS ROMS nested in climatology (1st exp.), WFS ROMS nested in NAT HYCOM temperature and salinity (2nd exp.) and WFS ROMS fully nested in NAT HYCOM (3rd exp.).

The symbol $|\cdot|$ represents the absolute value of the complex quantity.

High-frequency variations in all model simulations are close to the observed ones (Fig. 8), especially during winter. This agreement is attributed to the common wind forcing. The largest differences are observed in summer with climatological forcings. During June and July 2004, the southward current is overestimated in this model run while the model experiments with NAT HYCOM forcings produce a much more realistic current structure. This feature in the simulation with climatological boundary conditions is related to the temperature bias at station C11 shown in Fig. 7. The velocity RMS error is reduced by 0.04 m/s when NAT HYCOM boundary conditions are used instead of climatology. The currents are further improved with full nesting instead of only temperature and salinity. The model underestimates in general the strength of the currents, as it can be deduced from the regression coefficient. The strength of the currents on the shelf is however improved by nesting the model in NAT HYCOM.

At station C13 (Fig. 9), the bottom velocity of the WFS ROMS model with climatological forcing has a higher correlation coefficient and a better regression coefficient than the other model runs, but now the direction of the current is rotated to the observed currents by as much as 45°. As a consequence, the total RMS error for the WFS model forced by climatological boundary conditions is 0.073 m/s. Despite the large RMS error, the correlation coefficient is relatively high. This indicates that the main problem of this simulation is the mean current.

The use of NAT HYCOM temperature and salinity improves the phase error and reduce the RMS error. The full nesting provides the most accurate velocities in terms of RMS and phase. However, the correlation of this run is lower than the correlation obtained with the climatological boundary conditions.

4.3. HF radar currents

Two CODAR-type HF radar sites were operational during 2004: the sites at Redington Beach and Venice (see Fig. 1). The CODAR instruments operate with a 26 kHz frequency band centered at 4.55 MHz. The azimuthal resolution is 5° and the radial resolution is 6 km. We prefer to use the radial velocity field measured by each CODAR antenna for the model validation instead of the total currents since the total currents can only be deduced at the intersection of the range between both antennas. The radial velocity fields cover thus a larger area than the total velocities.

Both sites produce a radial velocity field at a hourly frequency since 28 April 2004. Since the model runs do not include tides, the tides must be subtracted from the HF radar data set. Based on all available CODAR data until 6 April 2006, tidal parameters of the radial velocity were determined using the T_TIDE package (Pawlowicz et al., 2002). Only the major constituents, i.e. O1, K1, M2 and S2 were included in this analysis. The present study is the first model validation for the WFS using the CODAR data of the Redington Beach and Venice site. We tested the

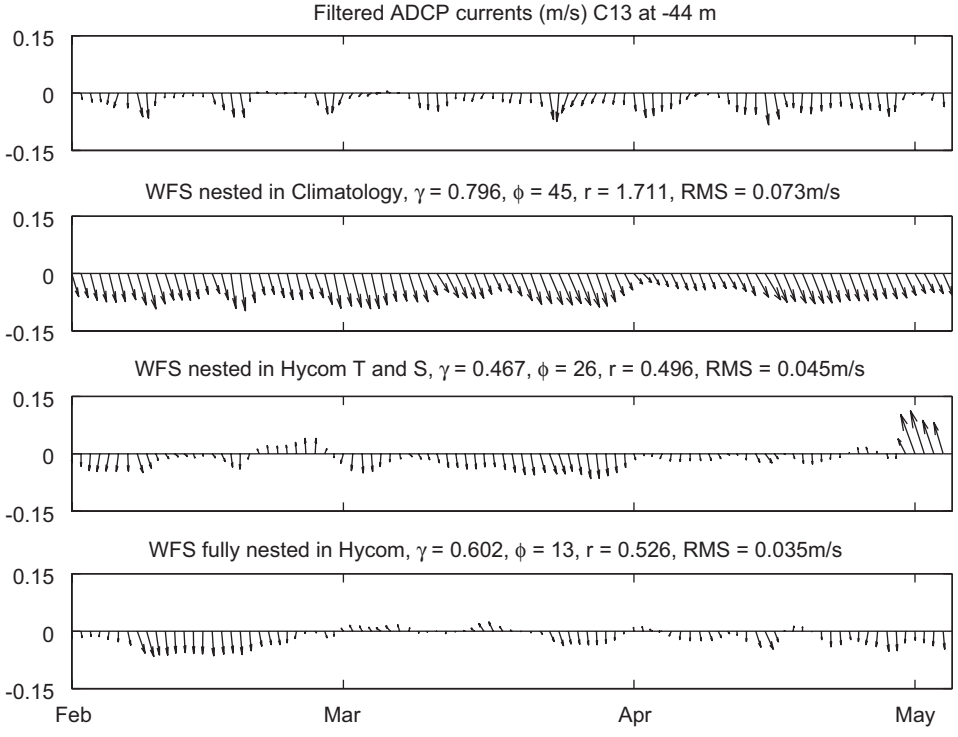

Fig. 9. Observed ADCP current time series (24-h low-pass filtered) of station C13 at 44 m depth and temperature of the WFS ROMS nested in climatology (1st exp.), WFS ROMS nested in NAT HYCOM temperature and salinity (2nd exp.) and WFS ROMS fully nested in NAT HYCOM (3rd exp.).

reliability of the CODAR data by comparing CODAR tidal amplitude V_r and phase ϕ_{v_r} to the parameters extracted from the ADCIRC tidal model (Mukai et al., 2001). ADCIRC provides the zonal tidal amplitude U' and phase ϕ'_u and the meridional amplitude V' and phase ϕ'_v. The corresponding radial tidal amplitude V'_r and phase ϕ'_{v_r} of ADCIRC were obtained by rotating the zonal and meridional parameters accordingly:

$$V_r'^2 = U'^2\sin^2\beta + V'^2\cos^2\beta - 2U'V'\sin\beta\cos\beta\cos\Delta\phi, \quad (12)$$

$$\phi'_{v_r} = \frac{\phi_u + \phi_v}{2} - \text{atan2}(\sin\Delta\phi(U'\sin\beta + V'\cos\beta), \times\cos\Delta\phi(U'\sin\beta - V'\cos\beta)), \quad (13)$$

where β at a given location is the angle between the North and the antenna (bearing), atan2 is the four quadrant inverse tangent and $\Delta\phi$ is the phase difference between the zonal and meridional tidal component:

$$\Delta\phi = \phi_u - \phi_v. \quad (14)$$

In general, the agreement between the CODAR and ADCIRC tidal parameters is good. Fig. 10 shows the amplitude and phase of the M2 tide at Redington Beach. A similar correspondence is found for the other tidal components and the other HF radar site. This agreement gives us confidence in the CODAR data for subsequent comparison of the sub-tidal currents of the three tested model configurations but it also shows some limitations of the CODAR observations: the accuracy is good near the antenna but it degrades with distance from the antenna and in some radial sectors the amplitude is underestimated, as it can be seen on Fig. 10.

The amplitudes of the M2 radial currents derived from CODAR are maximum at about 100 km off-shore from the HF radar antenna. This maximum is also present in the

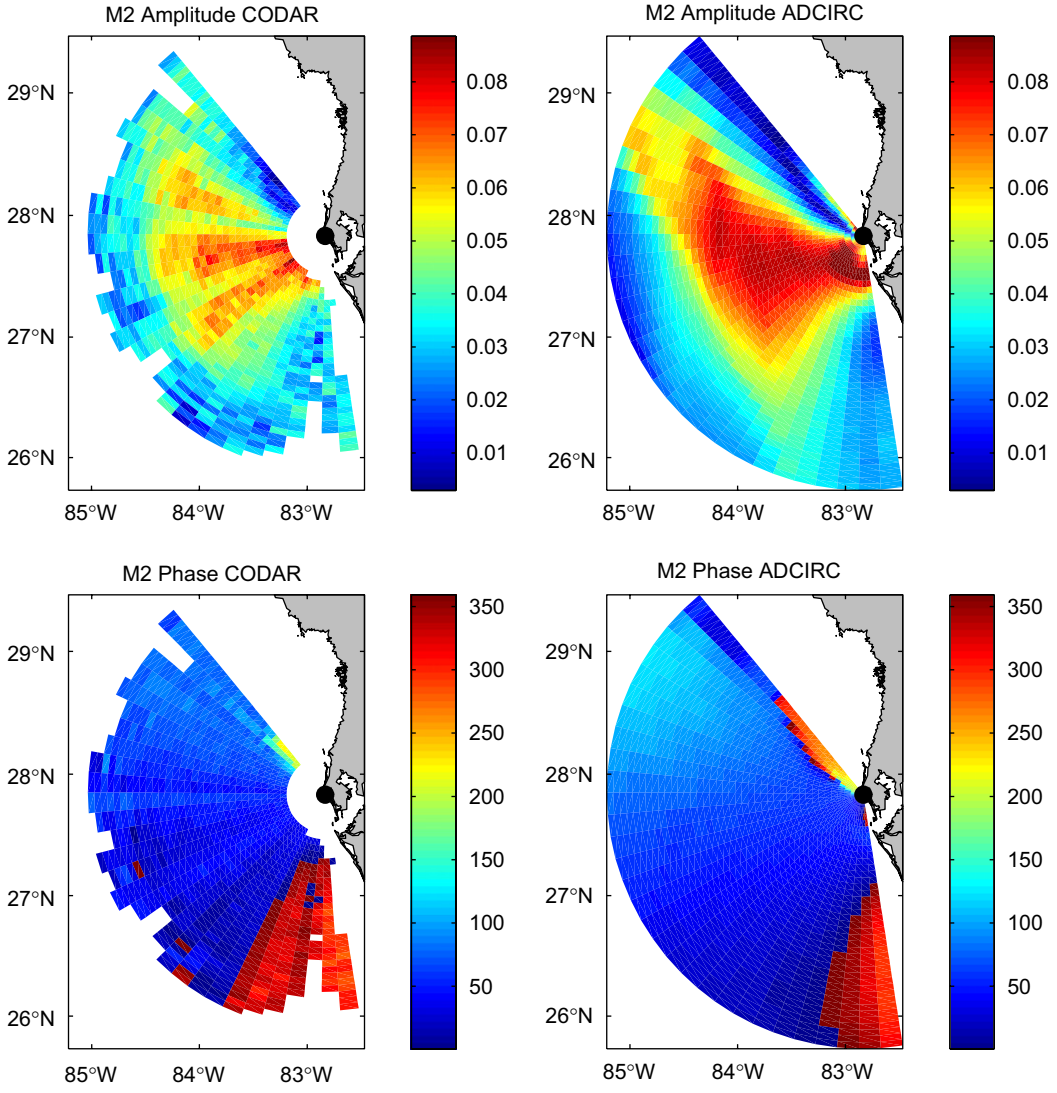

Fig. 10. M2 tidal amplitude (m/s) and phase (degrees) of the radial velocity at Redington Beach. The left panels show the results measured by CODAR and to the right are the results of the ADCIRC tidal model.

ADCIRC radial current. At this maximum, the radial direction is perfectly aligned with the major axis of the tidal current ellipse which is mostly perpendicular to the coastline in this region. At directions approximately parallel to the coastline, the CODAR antenna measures the minor axis of the tidal ellipse. This result is consistent with the tidal ellipses derived by He and Weisberg (2002a). At larger distances to the coast, the tidal currents decrease due to the topography.

The de-tided currents are averaged over two days to reduce the noise. Likewise, the velocity component of the three model configurations was averaged over two days, interpolated to the footprint of the two CODAR sites and rotated. The time averaged RMS difference between the three model runs and CODAR at the Redington site and Venice site is shown in Figs. 11 and 12, respectively. At the Redington site, all model simulations perform reasonably well within the first 100 km of the coast. Farther off-shore,

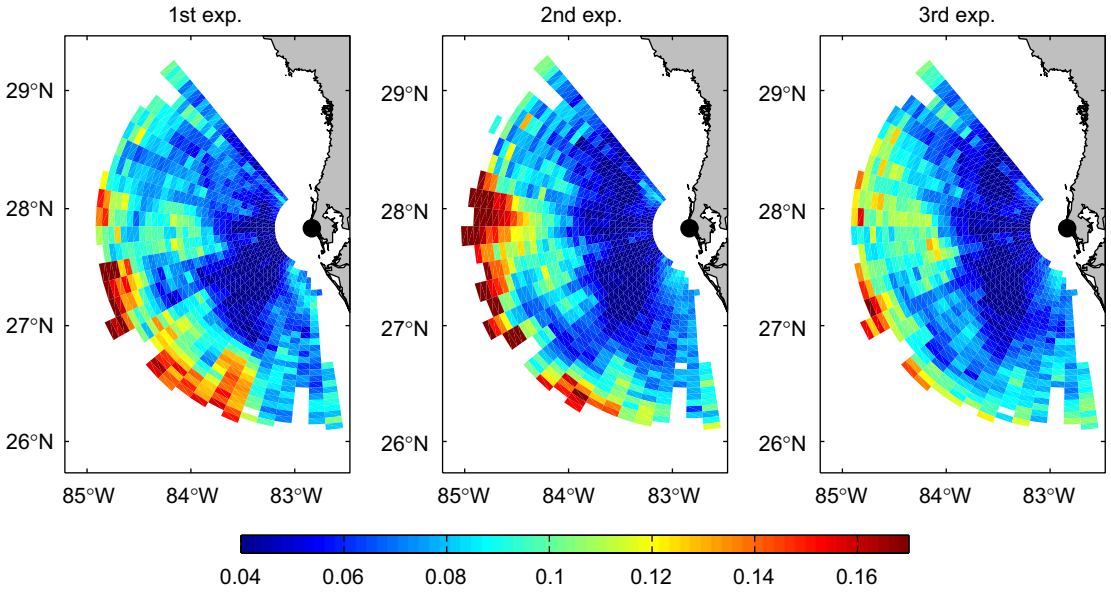

Fig. 11. The RMS difference (in m/s) between observed CODAR currents at Redington Beach station and radial currents of the WFS ROMS nested in climatology (1st exp.), WFS ROMS nested in NAT HYCOM temperature and salinity (2nd exp.) and WFS ROMS fully nested in NAT HYCOM (3rd exp.).

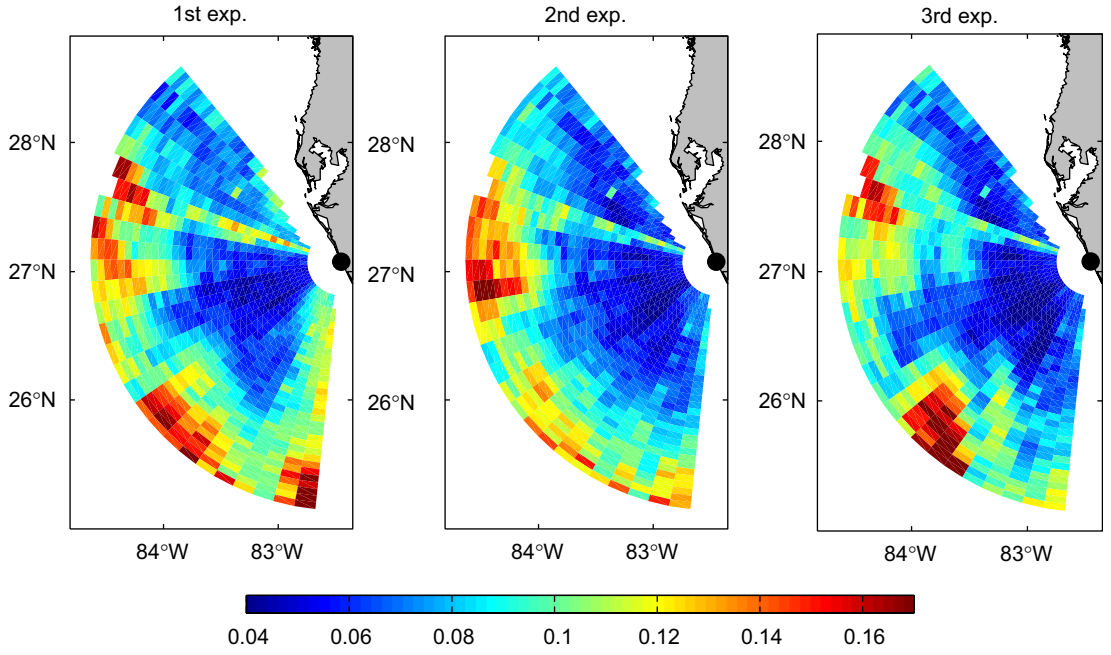

Fig. 12. The RMS difference between observed CODAR current Venice station and radial currents of the WFS ROMS nested in climatology (1st exp.), WFS ROMS nested in NAT HYCOM temperature and salinity (2nd exp.) and WFS ROMS fully nested in NAT HYCOM (3rd exp.).

the error increases partially due to the higher error in the CODAR data and due to the proximity of the shelf break, where the currents are more variable and to a lesser extent driven by winds as near-shore and thus more difficult to predict. Near the shelf break, the RMS errors of the simulation with climatological forcing are larger than 0.15 m/s (left panel of Fig. 11). This error is substantially reduced when ROMS is fully nested in NAT HYCOM (middle and right panels of Fig. 11). This indicates that the shelf slope and the outer shelf are affected by the open boundary conditions applied.

The RMS error patterns are similar at the Venice site (Fig. 12). On the inner shelf, the RMS error of all stations is comparable. On the outer shelf, the RMS error increases rapidly for the model simulation with climatological forcing. Unlike the Redington site, the velocity and elevation boundary conditions seem to have very little impact on the accuracy of the currents. This might be related to the fact that the shelf at the Venice site is slightly broader than at the Redington site.

The spatially averaged RMS errors for the Redington and Venice stations are given in Table 1. The findings in previous sections are confirmed by the CODAR measurements: the WFS ROMS fully nested in NAT HYCOM produces better results than the model forced with climatological boundary conditions. This improvement is mainly due to the more accurate temperature and salinity fields but also due to the information of surface elevation and transport at the boundary.

Table 1
Average RMS errors in m/s between the CODAR radial velocities at Redington Beach and Venice site and the three model configurations

Model run	Redington Beach	Venice
WFS nested in Climatology (1st exp.)	0.081	0.093
WFS nested in HYCOM T and S (2nd exp.)	0.081	0.083
WFS fully nested in HYCOM (3rd exp.)	0.073	0.082

Statistically, the model with NAT HYCOM boundary values performs thus better than the model with climatology. Fig. 13 illustrates the differences in the surface velocity at a particular time. This figure shows the radial velocity at Venice on June 23, 2004 and the corresponding fields for the model with climatological and NAT HYCOM boundary values. The velocity vectors of the model nested in climatology are depicted in Fig. 14. The LC in the model simulation with climatological boundary conditions does not enter and exit properly the model domain. This is due to the fact that the density gradient is too smooth and that the in- and outflow of the LC at the model boundary are not well represented. Furthermore the model simulation with this boundary condition develops filaments and small-scale circulation which can also be seen in the radial current (Fig. 13). The presence of these flow features does not agree with the currents measured by the HF-Radar antenna. In the fully nested case, the LC has a better defined path and this spurious circulation is not present.

5. Conclusions

The results of this work show that the boundary conditions have an influence not only on large-scale deep-ocean features such as the Loop Current (LC), but also on

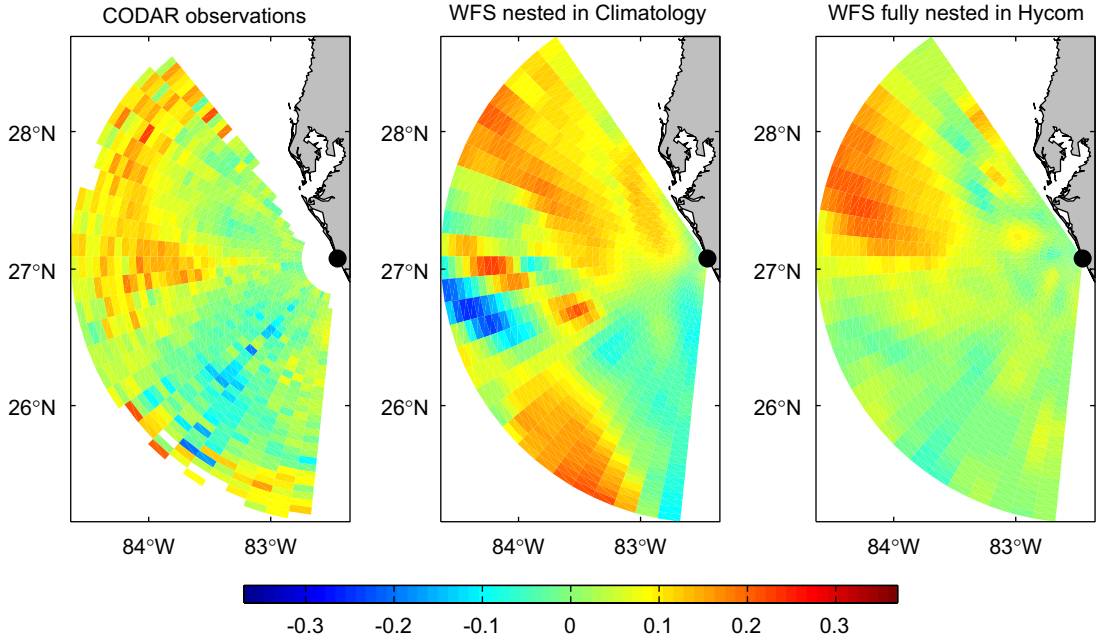

Fig. 13. Radial velocity (in m/s) measured from the CODAR antenna at Venice on May 23, 2004. The corresponding radial velocity WFS ROMS nested in climatology and fully nested in HYCOM are also shown. Positive values represent a current towards the antenna.

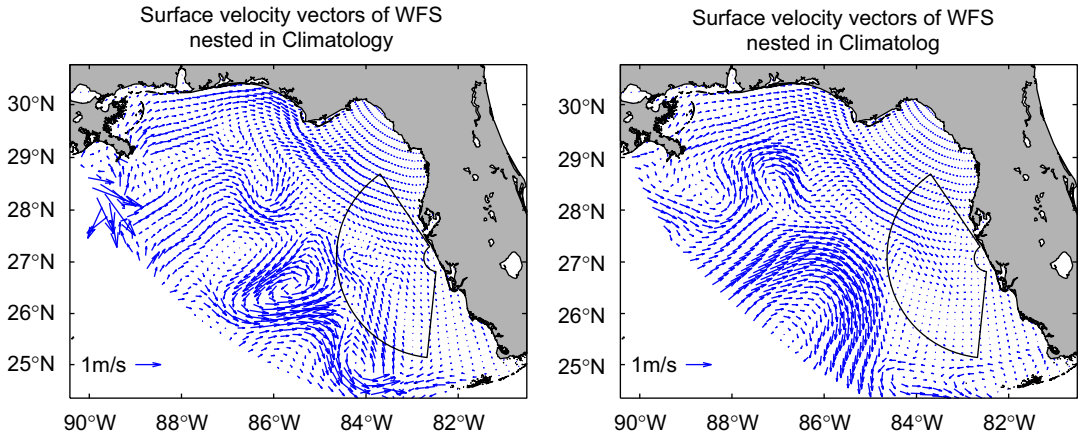

Fig. 14. Surface velocity on May 23, 2004 of WFS ROMS. The coverage of the CODAR antenna at Venice is also shown.

the shelf properties even if the open boundary is located in the deep ocean.

Gradients in the climatology appear to be too weak to support the LC with a realistic strength and path. Using NAT HYCOM temperature and salinity, the characteristics of the LC are much improved compared to climatological forcing but still weaker than the LC observed from altimetry. The best results concerning the LC position and strength were obtained if also the velocity and elevation are taken into account during the nesting.

Any model simulation forced only by temperature and salinity boundary conditions will not include the ageostrophic flow at the model boundary. The importance of the ageostrophic flow was assessed for the model simulation fully nested in HYCOM. The RMS difference between the model currents and the diagnosed geostrophic currents mimics the pattern of the LC. Using only temperature and salinity, the kinetic energy of the LC is underestimated by about 20%. The RMS difference between the model simulation with and without HYCOM elevation and velocity agrees with the magnitude and distribution of the ageostrophic flow variability.

On the shelf, stratification and currents are mainly conditioned by atmospheric heat and momentum fluxes. Although the atmospheric forcings are the same in all three experiments, the dynamics on the shelf differ and we were able to show that the choice of the boundary and initial conditions have a noticeable impact on the shelf solution. We showed that the climatological boundary values can create an unrealistic shelf current since the open boundary intersects the shallow isobaths.

The RMS error in ADCP and CODAR currents show that the velocity is also improved using NAT HYCOM boundary conditions. Consistent with SSH and temperature comparisons, the most accurate currents were obtained by the regional model which is fully nested in NAT HYCOM, i.e. not only temperature and salinity but also velocity and elevation are taken into account. Closer inspection of a particular time, showed that with climatological boundary conditions, the LC in- and outflow are not well represented and that in this simulation a spurious circulation from the LC affects the shelf.

Acknowledgements

This work was supported by the SouthEast US Atlantic Coastal Ocean Observing System (SEACOOS) program, the Global Ocean Prediction with the Hybrid Coordinate Ocean Model (HYCOM) program and the Coastal Ocean Data Assimilation Experiment (CODAE) of the US Office of Naval Research under the National Oceanographic Partnership Program (NOPP). We thank Ruoying He for providing the monthly temperature and salinity climatology. *In situ* data are attributed to the Ocean Circulation Group. Particular thanks go to Rick Cole, Jeff Donovan, Jay Law, Dennis Mayer, Cliff Merz, Vembu Subramanian and Jyotika Virmani. We also thank Sage Lichtenwalner for his help with the CODAR data. Sea level anomalies have been produced by the CLS Space Oceanography Division, Toulouse, France. The two anonymous reviewers are acknowledged for their careful revision and constructive criticism.

References

Alvera-Azcárate, A., Barth, A., Bouallègue, Z.B., Vandenbulcke, L., Rixen, M., Beckers, J.-M., 2007. Forecast verification of a 3D model of the Ligurian Sea. The use of Discrete Wavelet Transforms in the skill assessment of spatial forecasts. Journal of Marine Systems 65 (1–4), 460–483.

Bahurel, P., Dombrowsky, E., Lellouche, J.-M., the Mercator Project Team, 2004. Mercator Ocean Monitoring and Forecasting System, near-real-time assimilation of satellite and in situ data in different operational ocean models. In: Marine Environmental Monitoring and Predictions. 37th Liège Colloquium.

Barnier, B., Siefridt, L., Marchesiello, P., 1995. Thermal forcing for global ocean circulation model using a 3-year climatology of ECMWF analyses. Journal of Marine Systems 6, 363–380.

Barron, C.N., Kara, A.B., Martin, P.J., Rhodes, R.C., Smedstad, L.F., 2006. Formulation, implementation and examination of vertical coordinate choices in the Global Navy Coastal Ocean Model (NCOM). Ocean Modelling 11 (3–4), 347–375.

Bell, M., Forbes, R.M., Hines, A., 2000. Assessment of the FOAM global data assimilation system for real-time operational ocean forecasting. Journal of Marine Systems 25, 1–22.

Bertino, L., Lisæter, K.A., Counillon, F., Winther, N., Kegouche, I., Parouty, S., 2006. The TOPAZ monitoring and prediction system for the Atlantic and Arctic. In: Dahlin, H., Flemming, N.C., Marchand, P., Pettersson, S.E., (Eds.), European Operational Oceanography: Present and Future. Proceedings of the Fourth International Conference on EuroGOOS, 6–9 June 2005, Brest, France, pp. 456–459.

Blumberg, A.F., Mellor, G.L., 1987. Three-Dimensional Coastal Ocean Models. A Description of a Three-dimensional Coastal Ocean Circulation Model. Coastal Estuarine Science Series. American Geophysical Union, pp. 208–233.

Chapman, D., 1985. Numerical treatment of cross-shelf open boundaries in a barotropic coastal ocean model. Journal of Physical Oceanography 15, 1060–1075.

Chassignet, E.P., Garraffo, Z.D., January 15–19, 2001. Viscosity parameterization and the Gulf Stream separation. In: Muller, P., Henderson, D. (Eds.), From Stirring to Mixing in a Stratified Ocean. Proceedings 'Aha Huliko'a Hawaiian Winter Workshop. University of Hawaii, pp. 37–41.

Chassignet, E.P., Hurlburt, H.E., Smedstad, O.M., Halliwell, G.R., Hogan, P.J., Wallcraft, A.J., Baraille, R., Bleck, R., 2007. The HYCOM (HYbrid Coordinate Ocean Model) Data Assimilative System. Journal of Marine Systems 65, 60–83.

Demirov, E., Pinardi, N., Fratianni, C., Tonani, M., Giacomelli, L., Mey, P., 2003. Assimilation scheme of the Mediterranean Forecasting System: operational implementation. Annales Geophysicae, 189–204.

Ducet, N., Le Traon, P.Y., Reverdin, G., 2000. Global high-resolution mapping of ocean circulation from TOPEX/Poseidon and ERS-1 and -2. Journal of Geophysical Research 105 (C8), 19477–19498.

Flather, R., 1976. A tidal model of the northwest European continental shelf. Mémoires de la Societe Royale des Sciences de Liège 6 (10), 141–164.

Halliwell, G.R., Kourafalou, V., Balotro, R., Chassignet, E.P., Garnier, V., Hogan, P., Wallcraft, A.J., Hurlburt, H., Semdstad, O.M., Weisberg, R.H., 2005. Sensitivity of HYCOM West Florida Shelf simulations to Vertical Coordinate and Vertical Mixing choices. Continental Shelf Research, Submitted for publication.

He, R., Weisberg, R.H., 2002a. Tides on the West Florida Shelf. Journal of Physical Oceanography 32, 3455–3473.

He, R., Weisberg, R.H., 2002b. West Florida Shelf circulation and temperature budget for the 1999 spring transition. Continental Shelf Research 22, 719–748.

He, R., Weisberg, R.H., 2003a. A Loop Intrusion Case Study on the West Florida Shelf. Journal of Physical Oceanography 33, 465–477.

He, R., Weisberg, R.H., 2003b. West Florida Shelf circulation and temperature budget for the 1998 fall transition. Continental Shelf Research 23, 777–800.

He, R., Weisberg, R.H., Zhang, H., Muller-Karger, F., W., H.R., 2003. A cloud-free, satellite-derived, sea surface temperature analysis for the West Florida Shelf. Geophysical Research Letters 30(15).

He, R., Liu, Y., Weisberg, R.H., 2004. Coastal ocean wind fields gauged against the performance of an ocean circulation model. Geophysical Research Letters 31, L14303.

Hetland, R.D., Hsueh, Y., Leben, R.R., Niiler, P.P., 1999. A Loop Current-Induced Jet Along the Edge of the West Florida Shelf. Geophysical Research Letters 26, 2239–2242.

Kundu, P.K., Allen, J.S., 1976. Some three-dimensional characteristics of low-frequency current fluctuations near the Oregon coast. Journal of Physical Oceanography 6, 181–199.

Leben, R.R., 2005. Altimeter-Derived Loop Current Metrics. In: Circulation in the Gulf of Mexico: Observations and Models, Geophysical Monograph Series, vol. 161. American Geophysical Union, pp. 181–201.

Levitus, S., Boyer, T.P., 1994. World Ocean Atlas 1994 Volume 4: Temperature. NOAA Atlas NESDIS 4, Washington, DC.

Levitus, S., Burgett, R., Boyer, T.P., 1994. World Ocean Atlas 1994 Volume 3: Salinity. NOAA Atlas NESDIS 3, Washington, DC.

Marchesiello, P., McWilliams, J., Shchepetkin, A., 2001. Open boundary condition for long-term integration of regional oceanic models. Ocean Modelling 3, 1–20.

Mukai, A.Y., Westerink, J.J., Luettich, R.A., 2001. Guidelines for Using the Eastcoast 2001 Database of Tidal Constituents within the Western North Atlantic Ocean, Gulf of Mexico and Caribbean Sea. Coastal and Hydraulic Engineering Technical Note.

Pawlowicz, R., Beardsley, B., Lentz, S., 2002. Classical Tidal Harmonic Analysis Including Error Estimates in MATLAB using T_TIDE. Computers and Geosciences.

Shchepetkin, A., McWilliams, J., 2005. The Regional Oceanic Modeling System: a split-explicit, free-surface, topography-following-coordinate ocean model. Ocean Modelling 9, 347–404.

Stammer, D., Chassignet, E.P., 2000. Ocean state estimation and prediction in support of oceanographic research. Oceanography 13, 51–56.

Taylor, K.E., 2001. Summarizing multiple aspects of model performance in a single diagram. Journal of Geophysical Research 106 (D7), 7183–7192.

Weisberg, R.H., He, R., 2003. Local deep-ocean forcing contributions to anomalous water properties of the West Florida Shelf. Journal of Geophysical Research 108 (C6), 3184.

Weisberg, R.H., Black, B.D., Li, Z., 2000. An upwelling case study on Florida's west coast. Journal of Geophysical Research 105 (C5), 11459–11469.

Weisberg, R.H., Zhenjiang, L., Muller-Karger, F., 2001. West Florida shelf response to local wind forcing: April 1998. Journal of Geophysical Research 106 (C12), 31239–31262.

Weisberg, R.H., He, R., Liu, Y., Virmani, J.I., 2005. Circulation in the Gulf of Mexico: Observations and Models. West Florida Shelf Circulation on Synoptic, Seasonal, and Interannual Time Scales, Geophysical Monograph Series, vol. 161. pp. 325–347.